Received: 20 October 2017 | Revised: 16 January 2018 | Accepted: 5 March 2018
DOI: 10.1002/eco.1974

RESEARCH ARTICLE

WILEY

Use of satellite leaf area index estimating evapotranspiration and gross assimilation for Australian ecosystems

Rong Gan[1,2] | Yongqiang Zhang[2] | Hao Shi[1] | Yuting Yang[2] | Derek Eamus[1,3] | Lei Cheng[2] | Francis H.S. Chiew[2] | Qiang Yu[1]

[1] School of Life Sciences, University of Technology Sydney, Ultimo, NSW 2007, Australia

[2] CSIRO Land and Water, GPO Box 1700, ACTON, Canberra 2601, Australia

[3] Plant Biology and Climate Change Cluster, University of Technology Sydney, PO Box 123, Broadway, Ultimo, NSW 2007, Australia

Correspondence
Yongqiang Zhang, CSIRO Land and Water, Clunies Ross Street, Canberra 2601, Australia.
Email: yongqiang.zhang@csiro.au

Abstract

Accurate quantification of terrestrial evapotranspiration and ecosystem productivity is of significant merit to better understand and predict the response of ecosystem energy, water, and carbon budgets under climate change. Existing diagnostic models have different focus on either water or carbon flux estimates with various model complexity and uncertainties induced by distinct representation of the coupling between water and carbon processes. Here, we propose a diagnostic model to estimate evapotranspiration and gross primary production that is based on biophysical mechanism yet simple for practical use. This is done by coupling the carbon and water fluxes via canopy conductance used in the Penman–Monteith–Leuning equation (named as PML_V2 model). The PML_V2 model takes Moderate Resolution Imaging Spectrometer leaf area index and meteorological variables as inputs. The model was tested against evapotranspiration and gross primary production observations at 9 eddy-covariance sites in Australia, which are spread across wide climate conditions and ecosystems. Results indicate that the simulated evapotranspiration and gross primary production by the PML_V2 model are in good agreement with the measurements at 8-day timescale, indicated by the cross site Nash–Sutcliffe efficiency being 0.70 and 0.66, R^2 being 0.80 and 0.75, and root mean square error being 0.96 mm d^{-1} and 1.14 μmol m^{-2} s^{-1} for evapotranspiration and gross primary production, respectively. As the PML_V2 model only requires readily available climate and Moderate Resolution Imaging Spectrometer vegetation dynamics data and has few parameters, it can potentially be applied to estimate evapotranspiration and carbon assimilation simultaneously at long-term and large spatial scales.

KEYWORDS

canopy conductance, eddy covariance, evapotranspiration, gross primary production, modelling

1 | INTRODUCTION

The critical biophysical link between terrestrial water and carbon cycle is stomatal aperture. At leaf level, it not only regulates water vapour diffusion from leaves to the atmosphere (transpiration) but also controls plant fixation of carbon dioxide (CO_2) from the atmosphere through photosynthesis (carbon assimilation) simultaneously (Baldocchi, Luxmoore, & Hatfield, 1991). At ecosystems level, evapotranspiration (ET) and gross primary production (GPP) play vital roles in determining the global water and carbon balance (Beer et al., 2010; Jasechko et al., 2013). The degree of stomatal control on these water and carbon fluxes is quantified by bulk stomatal conductance (i.e., canopy conductance), estimate of which yet remains a major challenge for accurate estimate of ET and GPP (Kelliher, Leuning, Raupach, & Schulze, 1995).

Over decades, coupled carbon-water models based on diverse structure and parameterization schemes have been developed to estimate canopy conductance (G_c) for such purpose. They can roughly be classified into two groups. One is the "top-down" method, which utilizes observed water and carbon exchanges to deduce G_c directly (Baldocchi et al., 1991; Granier, Biron, & Lemoine, 2000; Stewart, 1988; Yebra, Van Dijk, Leuning, & Guerschman, 2015; Yebra, Van Dijk, Leuning, Huete, & Guerschman, 2013). Due to the lack of consideration regarding the interrelated water and carbon processes, these models have difficulties in interpreting the underlying mechanism and uncertainties in predictions. The other one is "bottom-up" upscaling approach, which usually integrates individual leaf stomatal response to environmental and physiological controlling factors up to canopy scale (Bonan, Oleson, Fisher, Lasslop, & Reichstein, 2012; Bonan, Williams, Fisher, & Oleson, 2014; Cox, Huntingford, & Harding, 1998; Dai et al., 2004; Running & Coughlan, 1988; Sellers, 1997; Tuzet, Perrier, & Leuning, 2003; Wang et al., 2011). Models developed in this way tend to imply mechanistic equations to represent water loss and carbon fixation interactively from leaves to canopy, from stand to regional scales. Although these process-based models are widely used, the relatively high complexity turns out to impede general application, and the performance can vary greatly across spatiotemporal scales (Bonan et al., 2014; De Kauwe et al., 2015; Morales et al., 2005; Wang et al., 2011). Therefore, credible and feasible modelling scheme of water and carbon fluxes is still highly required, and representation of a practical yet biophysically based G_c model remains elusive.

Numerous models have been developed to estimate ET (Bastiaanssen, Menenti, et al., 1998; Bastiaanssen, Pelgrum, et al., 1998; Cleugh, Leuning, Mu, & Running, 2007; Guerschman et al., 2009; Leuning, Zhang, Rajaud, Cleugh, & Tu, 2008; Long & Singh, 2012; McVicar & Jupp, 2002; Mu, Heinsch, Zhao, & Running, 2007; Norman, Kustas, & Humes, 1995; Yang, Long, & Shang, 2013; Zhang, Chiew, Zhang, & Li, 2009) and GPP (Hu et al., 2017; Ma et al., 2014; Running et al., 2004; Yang, Donohue, McVicar, & Roderick, 2015; Yebra et al., 2015) from stand to regional and global scale during the past few decades. On the one hand, the Penman–Monteith (PM) equation (Monteith, 1965)-based ET models have been proven as biophysically solid, which is often applied in combination with land surface information (e.g., radiation and vegetation) derived from remotely sensed imageries (Cleugh et al., 2007; Leuning et al., 2008; Mallick et al., 2015; Morillas et al., 2013; Mu, Zhao, & Running, 2011; Zhang et al., 2017; Zhang et al., 2016). However, carbon flux and the corresponding stomatal response are usually neglected in these models, which could induce uncertainties regardless of structure and conductance formulation (Liu, Wu, & Wang, 2017). On the other hand, to couple carbon and water fluxes, biochemical photosynthesis models (Collatz, Ball, Grivet, & Berry, 1991; Farquhar & von Caemmerer, 1892) are commonly incorporated into stomatal conductance (g_s) models (e.g., Ball–Berry model; Ball, Woodrow, & Berry, 1987; Collatz et al., 1991; Jarvis, 1976; Leuning, 1995; Medlyn et al., 2011; Stewart, 1988; Tuzet et al., 2003) to obtain G_c and thereby simulate ET and GPP in earth system schemes (Bonan et al., 2012; Kowalczyk, Wang, & Law, 2006; Sellers et al., 1996). Additionally, there are also models that implies empirical carbon uptake function together with conductance models, where GPP is calculated by simply multiplying light use efficiency with environmental constraints (Hu et al., 2017; Liu et al., 2017). These coupled model structure can vary greatly according to the principles applied to conceptualize the canopy structural (e.g., big-leaf or multilayer) and physiology (e.g., sunlit and shaded) properties, as well as the photosynthesis model used to estimate assimilation rate (Wang & Dickinson, 2012; Zhu et al., 2016). As a result, evaluation of the model uncertainty in ET and GPP estimates remains difficult and application problematic.

Recognizing the relative advantages of satellite-based PM model in estimating ET and the common employment of photosynthesis model in combination with g_s model, this study therefore explores the possibility of developing a relatively simple yet physiologically based model that couples water and carbon flux into G_c to calculate ET and GPP simultaneously. The coupled model should be easily applicable using readily available environmental variables as model inputs only and have few parameters that are easy to be parameterized, yet maintain basic physiological fundamentals. To achieve this, a Ball–Berry g_s model developed by Yu, Goudriaan, and Wang (2001) and Yu, Zhang, Liu, and Shi (2004) and a hyperbola assimilation formula by Thornley (1976) is incorporated and integrated to derive a novel G_c model, which is then introduced into a remotely sensed data-based PM model (Leuning et al., 2008; Zhang et al., 2016; Zhang et al., 2017). In this way, GPP can be calculated as canopy assimilation, and ET can be calculated from PM equation, respectively. The objectives of this study are as follows:

1. Upscaling the assimilation and g_s model to obtain the coupled G_c model that is then introduced to the PM equation;
2. Applying this simple coupled model together with remotely sensed leaf area index (LAI) to simulate ET and GPP; and
3. Using carbon and water flux observations at flux towers to test the model performance.

2 | MODEL DEVELOPMENT

2.1 | PML model and canopy conductance

The two main components of terrestrial ET are transpiration from vegetation canopy (E_t) and evaporation from soil surface (E_s). Among the satellite-based ET models (Cleugh et al., 2007; Leuning et al., 2008; Mu et al., 2007, 2011), the Penman–Monteith–Leuning (PML) model (Leuning et al., 2008) has routinely been used to estimate terrestrial ET and its components as a process-based approach (Zhang et al., 2017, 2016; Zhou, Zhang, Vaze, Lane, & Xu, 2015). Hence, the PML model is used in this study as the prototype to develop a coupled water and carbon model. In the PML model, E_c and E_s are explicitly accounted for in the form of latent heat flux (λE) following:

$$\lambda E = \lambda E_c + \lambda E_s, \tag{1}$$

$$\lambda E_c = \frac{\varepsilon Q_{A,c} + (\rho c_p/\gamma) D_a G_a}{\varepsilon + 1 + G_a/G_c}, \tag{2}$$

$$\lambda E_s = \frac{f \varepsilon Q_{A,s}}{\varepsilon + 1}, \tag{3}$$

where λ is the latent heat of evaporation (MJ kg^{-1}), Q_A is the total available energy (W m^{-2}), which is partitioned into canopy ($Q_{A,c}$), and soil ($Q_{A,s}$) available energy according to $\tau = exp(-k_A{\cdot}LAI)$, where $\tau = Q_{A,s}/Q_A$, k_A is extinction coefficient of Q_A and LAI is leaf area index derived from satellite imageries (Fisher, Tu, & Baldocchi, 2008; Leuning et al., 2008). In this model, transpiration is calculated by applying the PM equation exclusively to the canopy (Equation 2), where ε is the ratio of slope of the curve relating saturation water vapour pressure to temperature (Δ, kP$_a$ °C^{-1}) over the psychrometric constant (γ, kP$_a$ °C^{-1}), ρ is the air density (kg m^{-3}), D_a is the water vapour pressure deficit (VPD) of the air (kPa), G_a is the aerodynamic conductance (m s $^{-1}$), which is estimated following Leuning et al. (2008), and G_c is the canopy conductance to water vapour (m s^{-1}).

Yet no carbon flux is explicitly taken into account in the PML model, the parameter G_c in Equation 2 provides the vital connection between plant biophysical process (i.e., stomatal control) and the environmental variables (e.g., solar radiation and humidity; Hirose, 2005; Kelliher et al., 1995; Leuning et al., 2008), which can be calculated as

$$G_c = \frac{g_{s,\max}}{k_Q} ln\left\{\frac{Q_h + Q_{50}}{Q_{50}\exp(-k_Q LAI) + Q_{50}}\right\}\frac{1}{1 + D_a/D_{50}}, \tag{4}$$

where $g_{s,max}$ is the maximum stomatal conductance of the leaves at the top of the canopy (m s^{-1}), Q_h is the photosynthetically active radiation (PAR; W m^{-2}), k_Q is the extinction coefficient of PAR, Q_{50}, and D_{50} are the canopy absorbed PAR (W m^{-2}) and VPD (kPa) when $g_s = g_{s,max}/2$, respectively. This formulation of G_c is integrated from leaf level stomatal response to PAR only, with the carbon flux neglected and other environmental conditions assumed optimal. Detailed deduction of Equation 4 can be found in Kelliher et al. (1995) and Leuning et al. (2008).

Soil evaporation (E_s) in Equation 3 is calculated by reducing the Priestley–Taylor equilibrium evaporation (Priestley & Taylor, 1972) with a soil evaporation coefficient f that reflects the influence of water limitation on evaporation. A relatively robust formula developed by Zhang et al. (2010) is adopted in this study to estimate f as a variable controlled by precipitation and equilibrium evaporation (Fisher et al., 2008; Morillas et al., 2013; Zhang et al., 2010), which is expressed as

$$f_{Zhang} = \min\left\{\frac{\sum_{i-n}^{i} P_i}{\sum_{i-n}^{i} E_{eq,s,i}}, 1\right\}, \tag{5}$$

where n is the length of the "time lag" used to balance soil water content after precipitation, P_i is precipitation in the ith day (mm d^{-1}), $E_{eq.s.i}$ is the equilibrium E_s (mm d^{-1}). For each of the ith day in the time series, f is calculated as the accumulative proportion of precipitation to soil evaporative demand of the previous n days (Zhang et al., 2010). Because f is insensitive to variations in n, after a sensitivity analysis, n = 32 days is given in Equation 5 in this study.

2.2 | Coupled canopy conductance model

As mentioned above, carbon assimilation is not considered in Equation 4 for calculating the key parameter G_c. To estimate the closely coupled water and carbon fluxes, this study tries to formulate a novel G_c model that maintains biophysical meanings yet based on simple modelling framework for practical benefit. Following the upscaling principles, our canopy level G_c model is elaborated from leaf level g_s model and is given as follows:

$$G_c = \int_0^{LAI} g_s dl = m\frac{P_1}{k(P_2 + P_4)}\left\{kLAI + ln\frac{P_2 + P_3 + P_4}{P_2 + P_3\exp(kLAI) + P_4}\right\}\frac{1}{1 + D/D_0}, \tag{6}$$

where GPP is calculated as

$$GPP = A_{c,g} = \frac{P_1 C_a}{k(P_2 + P_4)}\left\{kLAI + ln\frac{P_2 + P_3 + P_4}{P_2 + P_3\exp(kLAI) + P_4}\right\}. \tag{7}$$

Detailed description of the G_c model and definition of each variable are illustrated in Appendix A.

Hence, a coupled G_c formula is obtained. This model can therefore be used to replace the original G_c equation (Equation 4) in the PML model to simulate ET, and GPP can be calculated by implementing Equation 7. The advantage of this coupled water and carbon PM model is that it requires routine environmental variables only for ET and GPP simulation and has a few free parameters that maintain the physiological significances of stomatal response and assimilation process. Owing to the capacity of estimating ecosystem carbon fixation and water loss at the same time, this model is herein named as PML_V2 model. A summary of the seven parameters in this model is given in Table 1.

3 | DATA AND METHODS

3.1 | Eddy covariance observations

The eddy covariance observations of energy, carbon, and water exchange have been widely used to interpret terrestrial ecosystem processes. The OzFlux (http://www.ozflux.org.au/) is part of the Australian Terrestrial Ecosystem Research Network and the global flux

TABLE 1 Details of seven parameters in the PML_V2 model

Parameter symbol	Definition	Unit	Allowed range
α	Initial slope of the light response curve to assimilation rate (i.e., quantum efficiency)	μmol CO$_2$ (μmol *PAR*)$^{-1}$	0.01–0.07
η	Initial slope of the CO$_2$ response curve to assimilation rate (i.e., carboxylation efficiency)	μmol m^{-2} s^{-1} (μmol m^{-2} s^{-1})$^{-1}$	0.01–0.07
m	Stomatal conductance coefficient	unitless	2–20
$V_{m,25}$	Notional maximum catalytic capacity of Rubisco per unit leaf area at 25 °C	μmol m^{-2} s^{-1}	10–120
D_0	Water vapour pressure deficit of the air	kPa	0.5–1.5
k_Q	Extinction coefficient of PAR	unitless	0.1–1
k_A	Extinction coefficient of available energy	unitless	0.5–0.8

network (https://fluxnet.ornl.gov/). Within Australian continent, OzFlux provides continuous micrometeorological measurements of over 30 flux sites that cover most Australian climate range and ecosystem types (Isaac et al., 2016). This provides us the excellent data set for model development and testing for the distinct Australian ecosystems.

Observations of water and carbon flux at nine flux sites in OzFlux network were used to evaluate the proposed PML_V2 model (Figure 1). The following criteria were used to filter available flux sites and measurements: (a) The flux site should have more than 2 years of continuous observations (since 2000), (b) observations of low confidence were excluded, and the reliable data should be more than 80% within each year at each site, (c) half-hourly observations of each variable were filtered to obtain daytime measurements only and further processed to obtain daily observations, and (d) the flux sites with satisfactory energy balance closure were selected, where the net radiation (R_n), soil heat flux (G), λE, and sensible heat flux (H) were used to calculate the energy balance ratio EBR = $(\lambda E + H)/(R_n - G)$, and the sites with overall EBR value greater than 70% were treated as satisfactory (Wilson et al., 2002). Night time observations were eliminated using the incoming shortwave radiation (R_s) greater than 20 W m^{-2} to avoid micrometeorological and instrument uncertainties (Ershadi, McCabe, Evans, Chaney, & Wood, 2014; Isaac et al., 2016). Daytime GPP was calculated as the difference of observed net ecosystem exchange and daytime ecosystem respiration (R_d), where R_d is estimated from observed night time ecosystem respiration (Bruhn et al., 2011; Papale et al., 2006; Reichstein et al., 2005; Shi et al., 2014). The GPP calculated from this algorithm was used as the observed GPP_{obs} for model use. The daily data set is further aggregated to obtain 8-day average values in accordance with the temporal resolution of remote sensed LAI (Hu et al., 2017; Papale & Valentini, 2003; Shi et al., 2014).

In total, nine Australian flux sites with 45 site-years (482 site-months) of in situ eddy covariance measurements were selected at last for further analysis. These sites represent a wide range of Australian climate regions from tropical to temperate and across five different plant functional types, including three savannas, one woody savanna, two grasslands (GRA), one open shrub land (OSH), and two evergreen broadleaf forests. Site details are presented in Table 2.

In situ eddy covariance energy flux data were eliminated when λE observations were negative and $||R_n - G| - |H + \lambda E|| > 250$ W m^{-2} to ensure the surface energy balance closure (Cleugh et al., 2007; Leuning et al., 2008; Wilson et al., 2002). Consequently, the observed λE is used in the parameterization and evaluation of the PML_V2 model.

3.2 | Remotely sensed data

Remotely sensed LAI with the temporal resolution of 8 days and the spatial resolution of 1 km was acquired from Moderate Resolution

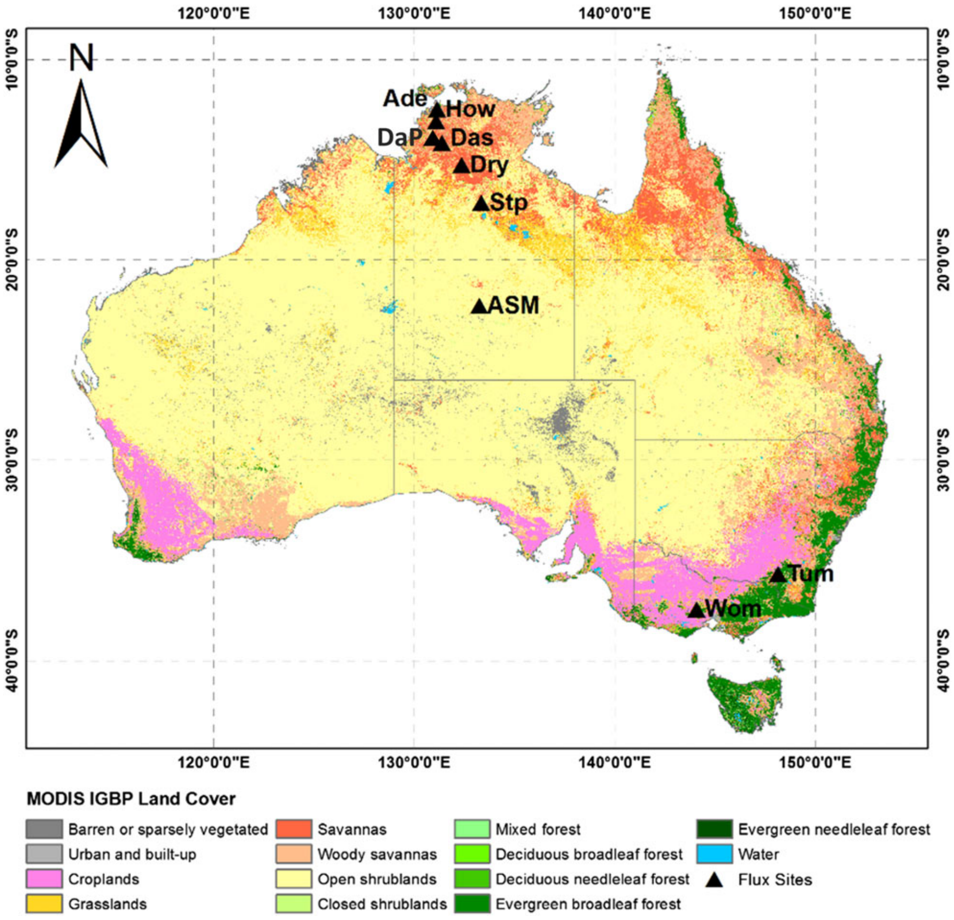

FIGURE 1 The International Geosphere–Biosphere Programme (IGBP) land cover type classification across Australia and locations of the nine flux sites used in this study. Remote sensing land cover data were downloaded from Moderate Resolution Imaging Spectrometer MCD12Q1 product

TABLE 2 Details of the nine Australian flux sites selected in this study

Site code	Site name	Climate[a]	PFTs	S	E	Canopy height (m)	Annual precipitation (mm/year)	T_{air}(° C)	LAI ($m^2\ m^{-2}$)	Period	Reference
				Latitude	Longitude			Range	Range	Start–end (year)	
AU-ASM	Alice Springs Mulga	TR	OSH	−22.28	133.25	6.5	306	−4–46	0.18–0.61	2011–2012	Cleverly et al. (2013)
AU-Ade	Adelaide River	TR	SA	−13.08	131.12	16.4	1,730	16–36	0.60–1.74	2007–2008	Beringer et al. (2016)
AU-DaP	Daly River Pasture	TR	GRA	−14.06	131.32	1.8	1,250	15–31	0.53–3.68	2007–2012	Beringer et al. (2016)
AU-Das	Daly River Uncleared	TR	SA	−14.16	131.39	16.4	1,170	12–37	0.72–2.00	2007–2012	Beringer et al. (2016)
AU-Dry	Dry River	TR	SA	−15.26	132.37	0.15	895	14–37	0.82–1.65	2010–2012	Beringer et al. (2016)
AU-How	Howard Springs	TR	WSA	−12.50	131.15	16	1,700	20–33	0.76–2.36	2004–2012	Beringer et al. (2016)
AU-Stp	Sturt Plains	TR	GRA	−17.15	133.35	0.5	640	11–39	0.23–1.02	2010–2012	Beringer et al. (2016)
AU-Tum	Tumbarumba	T	EBF	−35.66	148.15	40	1,000	−10–30	2.72–5.52	2001–2012	Leuning, Cleugh, Zegelin, and Hughes (2005)
AU-Wom	Wombat State Forest	T	EBF	−37.42	144.09	25	650	1–30	3.24–5.32	2011–2012	Van Gorsel et al. (2016)

[a] Climate is categorized into tropical (TR) and temporal (T).

Imaging Spectroradiometer (MODIS) products (MOD15A2; http://daac.ornl.gov). At each flux site, LAI data lie in the 3 km × 3 km centred grid matrix according to the flux coordinates was selected to obtain LAI time series. The 3 km × 3 km centred grid data are used to reduce the mismatch between the course MODIS pixels and the footprint size of the flux sites (Shi et al., 2014). The 8-day data were processed through quality control, interpolation, and filtering using the TIMESAT tool (Jönsson & Eklundh, 2004) to obtain high quality LAI for model use (Zhang & Wegehenkel, 2006).

Additionally, remote sensed ET from MOD16A2 and GPP from MOD17A2, with 8-day temporal resolution were downloaded from the Numerical Terradynamic Simulation Group (NTSG; http://www.ntsg.umt.edu), which were then extracted at each flux site for comparison with the PML_V2 modelled results.

3.3 | Evaluation of model performance

The global optimization method—genetic algorithm—in MATLAB® (The MathWorks, Inc.) was used to calibrate the PML_V2 model parameters at each flux site. A multi-objective cost function (F_{cost}) was set-up to maximize the sum of the Nash–Sutcliffe efficiency (NSE) between simulated and observed ET and GPP as

$$F_{cost} = NSE_{ET} + NSE_{GPP}, \tag{8}$$

$$NSE_{ET} = 1 - \frac{\sum_{i=1}^{N} \left| ET_{sim,i} - ET_{obs,i} \right|^2}{\sum_{i=1}^{N} \left| ET_{obs,i} - \bar{ET}_{obs} \right|^2}, \tag{9}$$

$$NSE_{GPP} = 1 - \frac{\sum_{i=1}^{N} \left| GPP_{sim,i} - GPP_{obs,i} \right|^2}{\sum_{i=1}^{N} \left| GPP_{obs,i} - \bar{GPP}_{obs} \right|^2}, \tag{10}$$

where subscripts *obs* and *sim* represent observation and simulation, respectively, *N* is the length of the 8-day time series at each site. Thus, estimates of ET and GPP using PML_V2 were evaluated using the NSE of 8-day ET and GPP, respectively. At each flux site, the four parameters are optimized by maximizing the grand cost function F_{cost} (Equations 8–10).

In addition to NSE, we also used the standard metrics for evaluating model performance, namely, the linear regression slope, the coefficient of determination (R^2), and the root mean square error (RMSE), as given below:

$$R^2 = \left(\frac{\sum_{i=1}^{N} \left(X_{sim,i} - \bar{X}_{sim} \right) \left(X_{obs,i} - \bar{X}_{obs} \right)}{\sqrt{\sum_{i=1}^{N} \left(X_{sim,i} - \bar{X}_{sim} \right)^2 \sum\limits_{i=1}^{N} \left(X_{obs,i} - \bar{X}_{obs} \right)^2}} \right)^2, \tag{11}$$

$$RMSE = \sqrt{\frac{1}{N} \sum_{i=1}^{N} \left(X_{sim,i} - X_{obs,i} \right)}, \tag{12}$$

where *X* represents the evaluated variable, either ET or GPP in this study. Higher slope, NSE and R^2, and lower RMSE indicates good model performance.

Two experiments were set to evaluate the ability of the model in estimating ET and GPP. First, the PML_V2 model was calibrated at each flux site using all available data individually. In this way, model performance and parameter variability are examined across sites. Second, the available data at each flux site were split into two equal parts, and each of the half data set was used to calibrate the model in turn. The predicted ET and GPP from the validation period was then accumulated to obtain continuous time series at each site as predictions. This experiment tests the robustness of the model in predicting ET and GPP.

4 | RESULTS

4.1 | Sensitivity analysis

Among the seven parameters (Table 1), previous studies have shown that D_0, k_Q, and k_A are insensitive parameters to estimate ET in the PML model (Leuning et al., 2008; Zhang, Chiew, Zhang, Leuning, & Cleugh, 2008). Similarly, we conducted a sensitivity analysis for all the parameters in the PML_V2 model. With all of the seven parameters optimized, the values ranged between 0.50–1.5 for D_0, 0.10–0.82 for k_Q, and 0.50–0.80 for k_A across the nine sites. However, when given $D_0 = 0.7$, $k_Q = 0.6$, and $k_A = 0.7$ as constants, we yield identical estimates for the rest four parameters (α, η, m, and $V_{m,25}$) and the statistics of simulated ET and GPP (data not shown). Thus, a similar conclusion was drawn that performance of the PML_V2 model is relatively insensitive to variations in D_0, k_Q, and k_A. Therefore, all the following results are presented with only the free parameters: α, η, m, and $V_{m,25}$ optimized in this study. Additionally, as the model is relatively insensitive to variations in the atmospheric CO_2 concentration and the observation is not readily available, C_a is given as 380 μmol mol $^{-1}$ despite the value can vary in reality. Because water and carbon fluxes are coupled via G_c (Section 2.2), the sensitivity of G_c to variations in α, η, m, and $V_{m,25}$ is herein examined as shown in Figure 2.

As can be seen from Figure 2, lower α results in a lower G_c and so does η. With α or η increasing to its upper limit (i.e., 0.07), the sensitivity of G_c to these two parameters reduces to a smaller degree than that of their lower limits. However, it is not the case for m, where G_c shows an equal variation degree within the allowed limits. As for $V_{m,25}$, variation in G_c within lower $V_{m,25}$ values (below 70 μmol m^{-2} s^{-1}) is much higher than that of larger $V_{m,25}$ range (70–120 μmol m^{-2} s^{-1}). Hence, the model performance is likely to be relatively sensitive in variations of the parameters η and m but less so in α and $V_{m,25}$. Further model experiment indicates that the parameterized values of η and m show a larger variation across biomes, which means that they are key parameters that control ET and GPP estimates in this model.

4.2 | Parameterization

For individual parameterization at each flux site, the optimized values of the four parameters are presented in Table 3. All of the parameters vary within a wide range across sites in general. The initial slopes of the assimilation response curves to light (α) and CO_2 (η) ranged between 0.05–0.07 (μmol CO_2 [μmol PAR]$^{-1}$) and 0.013–0.063 (μmol m^{-2} s^{-1} [μmol m^{-2} s^{-1}]$^{-1}$), respectively. Although α shows a relatively small variation among nine sites (average 0.067 μmol CO_2 [μmol PAR]$^{-1}$), smaller η values were detected at two forest sites (about 0.015 μmol m^{-2} s^{-1} [μmol m^{-2} s^{-1}]$^{-1}$) when compared with that of the nonforest sites in general (between 0.013–0.063 μmol m^{-2} s^{-1} [μmol m^{-2} s^{-1}]$^{-1}$). Besides, stomatal conductance coefficient (m) ranged from 5.75 to 20 across all biomes. In addition, $V_{m,25}$ also varied considerably from 34 μmol m^{-2} s^{-1} at DaP to 120 μmol m^{-2} s^{-1} at five different sites (Das, Dry, ASM, Tum, and Wom). However, no clear pattern was observed for the difference in m and $V_{m,25}$ values across biomes.

4.3 | Model calibration

Site-specific parameterization results are used to evaluate the model performance with the parameters α, η, m, and $V_{m,25}$ optimized. Figure 3 presents the statistics of simulated ET and GPP at 8-day temporal resolution when compared with observations. It can be seen that the model performs well in simulating both ET and GPP. Collectively, the model explains 80% and 71% of variations in ET and GPP, respectively, with the average NSE values at 0.71 for ET and 0.63 for GPP across biomes. This indicates a reasonably high degree of estimating water and carbon fluxes using the PML_V2 model. This is further evident from a large linear regression slope and lower RMSE values (Figure 3). Additionally, the PML_V2 model performed slightly better in 8-day ET estimates than GPP. On average, the model explains 9% higher of ET variation than that of GPP, yet with a much smaller difference in NSE (about 0.07). The lower slopes of GPP indicate that the algorithm tends to underestimate GPP by 20–40% across sites.

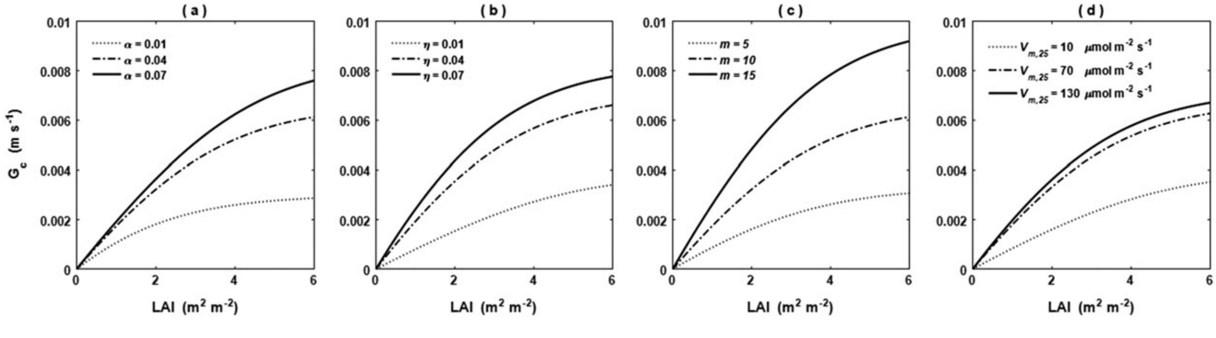

FIGURE 2 Response of G_c to (a) α, (b) η, (c) m, (d) $V_{m,25}$. Except when varied, parameter values are $\alpha = 0.04$, $\eta = 0.03$, $m = 10$, and $V_{m,25} = 50$ μmol m^{-2} s^{-1}. $R_s = 500$ W m^{-2}, PAR is assumed to be $0.45R_s$, $D = 1$ kPa, $D_0 = 0.7$ kPa, $Pa = 100$ kPa, $T_{air} = 25°C$, $C_a = 380$ μmol mol $^{-1}$, and $k_A = k_Q = 0.6$. LAI = leaf area index

TABLE 3 Optimized parameter values of the PML_V2 model at nine Australian flux sites

Site name	PFT	Optimized parameter values			
		α	η	m	$V_{m,25}$
ASM	OSH	0.07	0.026	5.7	120
Ade	SA	0.07	0.063	13.4	36
DaP	GRA	0.07	0.013	9.75	34
Das	SA	0.07	0.024	12.2	120
Dry	SA	0.07	0.020	8.6	120
How	WSA	0.07	0.028	16.5	108
Stp	GRA	0.07	0.022	20	82
Tum	EBF	0.06	0.014	14.7	120
Wom	EBF	0.05	0.015	12.6	120
Parameter range		0.01–0.07	0.01–0.07	2–20	10–100

[a] The model is calibrated by maximizing $NSE_{ET} + NSE_{GPP}$ using all available data at each site independently.

Except general good performance, the model can successfully capture seasonal variation in ET and GPP as well. The observed and simulated 8-day time series ET and GPP are presented in Figures 4 and 5 for each of the nine study sites, respectively. Result in Figure 4 indicates that the model is capable of reproducing seasonal pattern in actual ET; yet a slightly better performance can be found during higher precipitation periods when compared with that of lower precipitation periods for most sites. The higher consistency between simulated and observed ET is detected for forest sites (Tum and Wom) than nonforest sites throughout the year, especially during lower precipitation periods. Additionally, the PML_V2 model could also reproduce reasonably good temporal dynamics for GPP (Figure 5). Using observed GPP as benchmark, the best model performance was found at the grassland site DaP (NSE = 0.85), followed by the forest site Wom (0.79) and two savanna sites Das (R^2 = 0.74) and Ade (R^2 = 0.73). However, the least satisfactory model performance is at the grassland site Stp (R^2 = 0.59). The seasonal variation in GPP is tend to be overestimated during lower GPP periods where water availability (precipitation) is limited, especially for nonforest biomes (savanna, OSH and GRA).

4.4 | Model validation

Time series derived from the half-split validation experiment (Section 3.3) were used to evaluate the model robustness of predicting ET and GPP. For each of the nine sites, we split the data into half and used each half data for calibration and the remaining half for validation in turn. Thereby, the ET and GPP predictions during each of the half validation period are yield by applying the model with optimized parameters obtained from calibration period. Because the two parameter sets yield for each site are very close to those optimized with all data at the same site in general, the two half predictions are merged into a full time series at each site to evaluate model performance.

Collectively, the cross site average NSE, R^2 and slope are 0.70, 0.80, and 0.97 for 8-day ET and 0.61, 0.71, and 0.54 for 8-day GPP, respectively. RMSE is 0.95 mm d^{-1} for ET and 1.02 μmol m^{-2} s^{-1} or GPP across sites (data not shown). This result is very close to that of calibration (Figure 3). Figure 6 presents the model performance degradation from calibration to validation, as indicated by the statistical difference between the two at each site. As can be seen that there is only slight degradation found in both ET and GPP. NSE and R^2 of 8-day ET were nearly identical with that of model calibration, with the maximum difference of NSE found at Ade and Das; yet the overall RMSE increased less than 0.1 mm d^{-1}. Additionally, despite the minor degradation in R^2 value for 8-day GPP at most sites, maximum

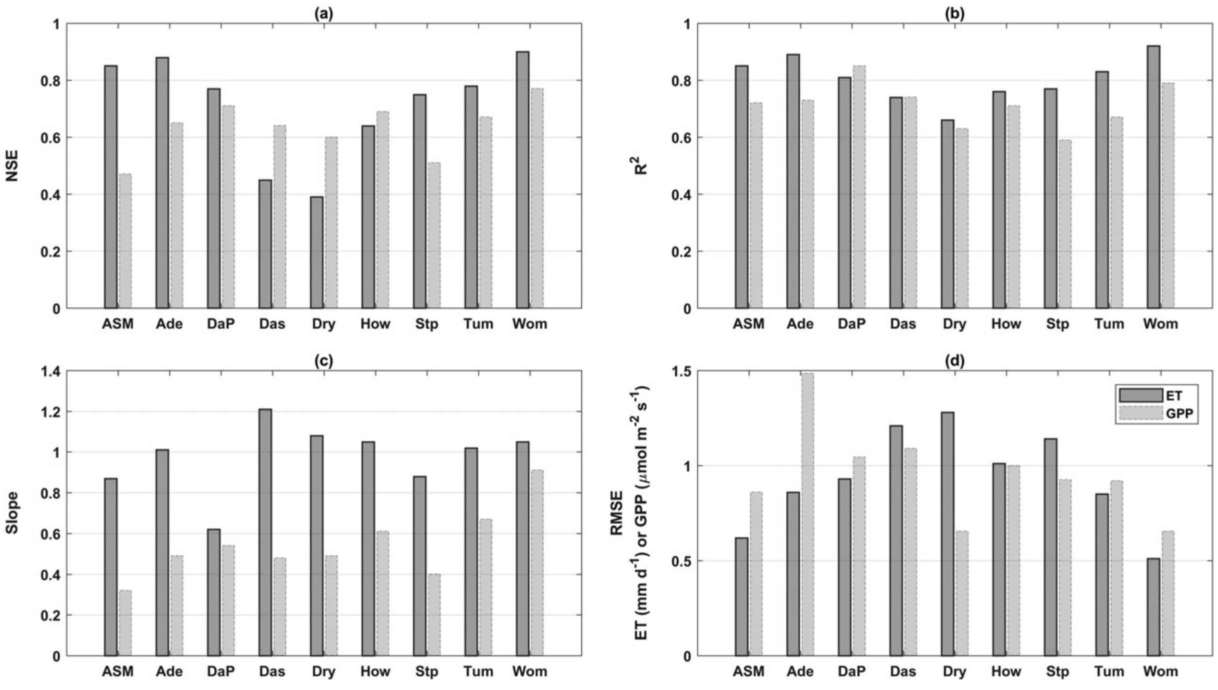

FIGURE 3 Statistics of model performance at 8-day time scale for ET and GPP estimates. The parameters are derived from independent optimization using all available data at each site. Nash–Sutcliffe efficiency (NSE), coefficient of determination (R^2), linear regression slope, and root mean square error (RMSE) of simulation against observation for both ET and GPP are presented

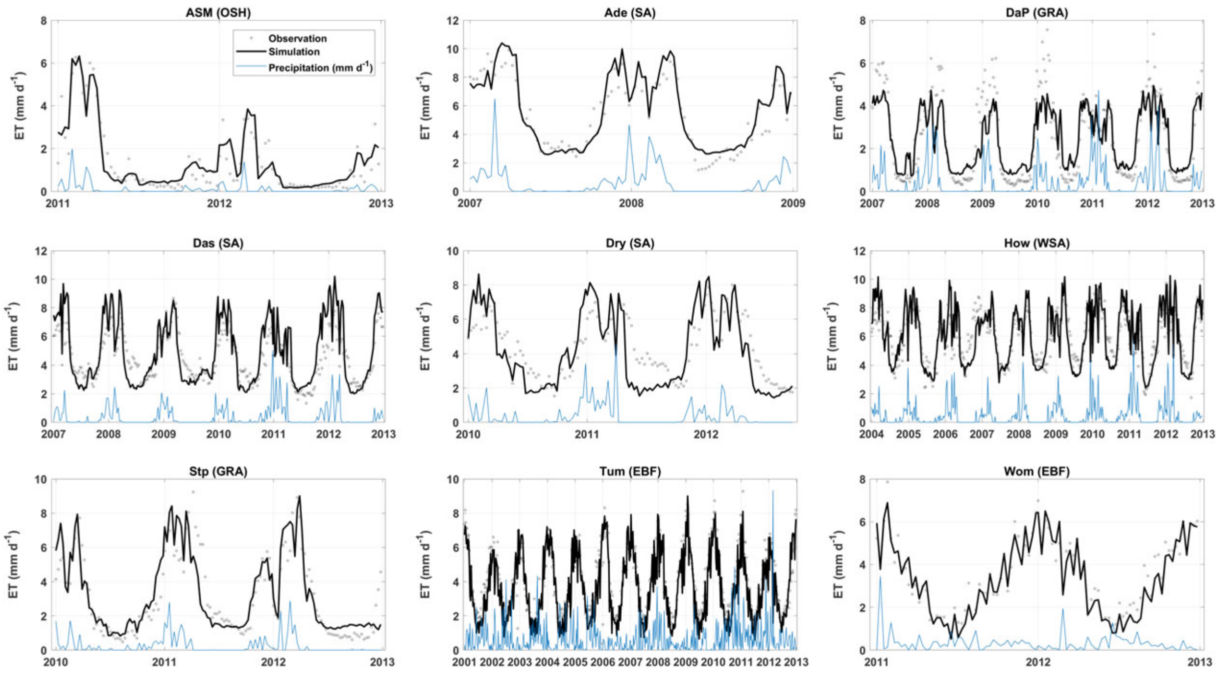

FIGURE 4 Time series of 8-day average ET and precipitation in mm d^{-1} at nine flux sites. Observed ET is derived from flux tower measurements. Simulated ET is yielded from PML_V2 with four parameters optimized at each site independently (Table 3)

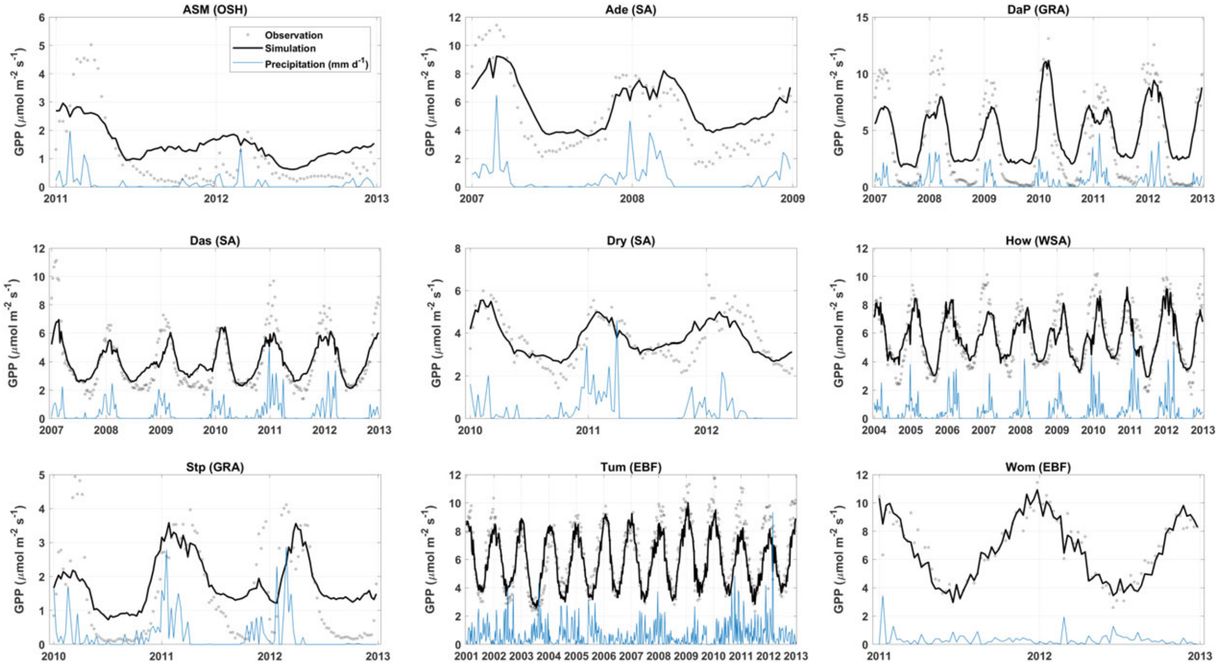

FIGURE 5 Time series of 8-day average GPP in μmol m^{-2} s^{-1} at nine flux site. Observed GPP is derived from flux tower measurements. Simulated GPP is yielded from PML_V2 with four parameters optimized at each site independently (Table 3)

decrease in NSE is found at ASM and Tum (0.05), followed by Ade (0.03) and Stp (0.02), and RMSE increased less than 0.12 μmol m^{-2} s^{-1} for all sites, which indicate a marginal degradation in general. Note that a better validation is detected for GPP at Stp in terms of R^2 and for ET at Tum in terms of RMSE; yet the difference is minor. This is caused by optimizing the Equation 8–10, where the optimal solution is achieved by compromising NSE between GPP and ET. When the ET validation increases, the GPP validation depredates to obtain better overall results. The overall results imply that the PML_V2 model is of high robustness in predicting both ET and GPP.

5 | DISCUSSION

5.1 | Model parameters

The values of the optimized parameters were comparable with previous studies. The average quantum efficiency α yield from PML_V2 (0.067 μmol CO_2 [μmol PAR]$^{-1}$) is consistent with the values in Yu et al. (2004). Results with the four parameters calibrated show that α is clearly different between forest and nonforest sites. Lower α values (about 0.58 μmol CO_2 [μmol PAR]$^{-1}$) in site Tum and Wom indicate

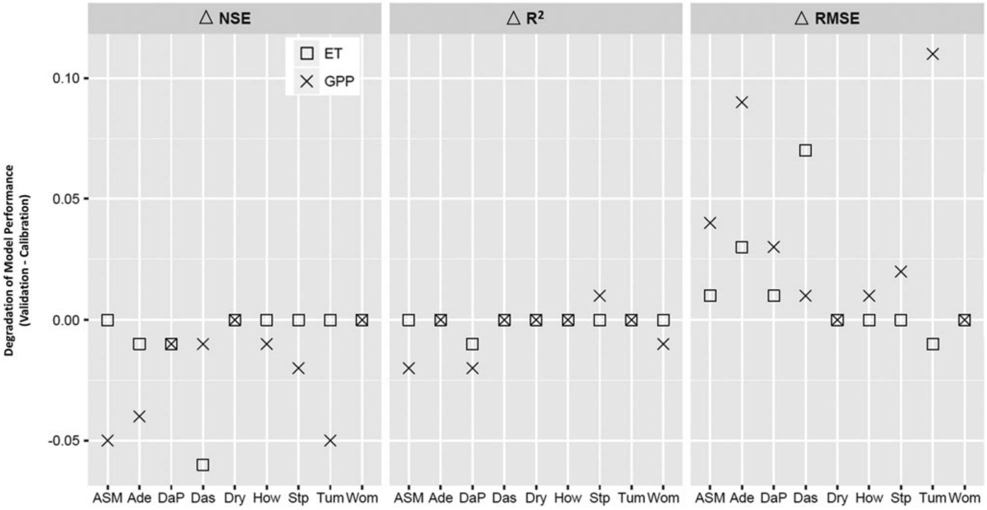

FIGURE 6 Degradation of model performance from calibration to validation at each of the nine sites. Statistics shown are the difference of R^2, Nash–Sutcliffe efficiency (NSE), and root mean square error (RMSE) as validation minus calibration, with the black and shaded symbols representing the values of ET and GPP, respectively

the heterogeneity in the radiation response in these energy-limited ecosystems, whereas higher α (0.070 μmol CO_2 (μmol PAR)$^{-1}$) at other sites represents a roughly similar pattern of light response among savanna, shrubs and grassland for their patchy vegetation cover. The estimated carboxylation efficiency η is generally lower in forest sites (about 0.015 μmol m^{-2} s^{-1} [μmol m^{-2} s^{-1}]$^{-1}$) and higher at nonforest sites (vary from 0.013 to 0.63 μmol m^{-2} s^{-1} [μmol m^{-2} s^{-1}]$^{-1}$). This implies that the woody ecosystem is relatively insensitive response to changes in CO_2 concentration than herbaceous ones. Meanwhile, the stomatal conductance coefficient *m* shows a wide variation across biomes, which all fall into the optimal range. In addition, smaller $V_{m,25}$ values were found in Ade, DaP, and Stp with all the rest sites having larger $V_{m,25}$ values. As canopy conductance became insensitive at high $V_{m,25}$ values (Figure 2), this could be a result of the fixed *a* and *b* given as a constants under 25and 41 °C in the model as mentioned above.

In the PML_V2 model, α was calibrated as a constant whereas in reality, it could change with water availability, being higher in the wet season but lower in the dry season as higher water availability usually induces higher quantum efficiency (Eamus et al., 2013). Further study is required to obtain α that varies against water factors such as precipitation or soil water content, to improve model performance in the dry season. Besides, we introduced a notional catalytic capacity $V_{m,25}$ into the model, which is different from the commonly used maximum carboxylation rate $V_{c,max}$; yet a similar optimal range was given for optimization (Bonan et al., 2012; Kattge & Knorr, 2007). Although $V_{m,25}$ has been adjusted to temperature accordingly, it should be noted that the obtained values are different from those of $V_{c,max}$. However, the model performance is relatively insensitive to variations of this parameter at 8-day temporal scale despite the leaf level internal control of conductance to photosynthesis (Chen, Liu, Cihlar, & Goulden, 1999).

5.2 | Comparison with MODIS products and other studies

The MODIS products are widely used to map global ET and GPP and compare with modelled results. We hereby conducted a brief comparison of the predicted results using PML_V2 model with that derived from MODIS product. MODIS ET (MOD15A2; ET_{MODIS}) and GPP (MOD17A2; GPP_{MODIS}) time series was extracted and processed at the nine study sites. The predicted ET and GPP from PML_V2 model was compared with ET_{MODIS} and GPP_{MODIS} at 8-day scale against observations as shown in Figure 7. As expected, MODIS products perform worse than PML_V2 model in general. Despite negative NSE values of MODIS (set to zero in Figure 7a,d), the average R^2 yield from MODIS products across sites is 0.68 for ET and 0.51 for GPP, which explains 12% and 22% less variations in ET and GPP when compared with PML_V2 model, respectively. Moreover, the RMSE values of PML_V2 are clearly lower than that of MODIS. Specifically, ET_{MODIS} tends to underestimate actual ET at nonforest sites (i.e., Ade, Das, Dry, How, ASM, and Stp), especially during low precipitation periods, but overestimates at forests (i.e., Tum and Wom) throughout the study period (data not shown). This suggests that it is hard to satisfactorily use the globally parameterized two MODIS products for Australian biomes, where the proposed PML_V2 model is of high reliability and robustness in ET and GPP estimate.

In addition, we also compared our modelled results with other two coupled models at sites where available, namely, How and Tum which are commonly used in the literature. Only the site-specific parameterization performance is used for fair comparison as given in Table 4. On average, the R^2 and RMSE of ET are better or about the same with that obtained by Hu et al. (2017) and Yebra et al. (2013), and GPP is closely comparable or better than the simulation yield by Hu et al. (2017) and Yebra et al. (2015) using their coupled model. This gives us confidence that the PML_V2 model proposed here is relatively simple yet reliable to estimate ET and GPP.

5.3 | Model uncertainty

The advantage of the PML_V2 model is, as described in the Equation 6, inclusion of both energy and carbon responses in a simple coupled formulation, which keeps the biological energy-driven mechanism and includes CO_2 as an independent environmental constraint (Kelliher

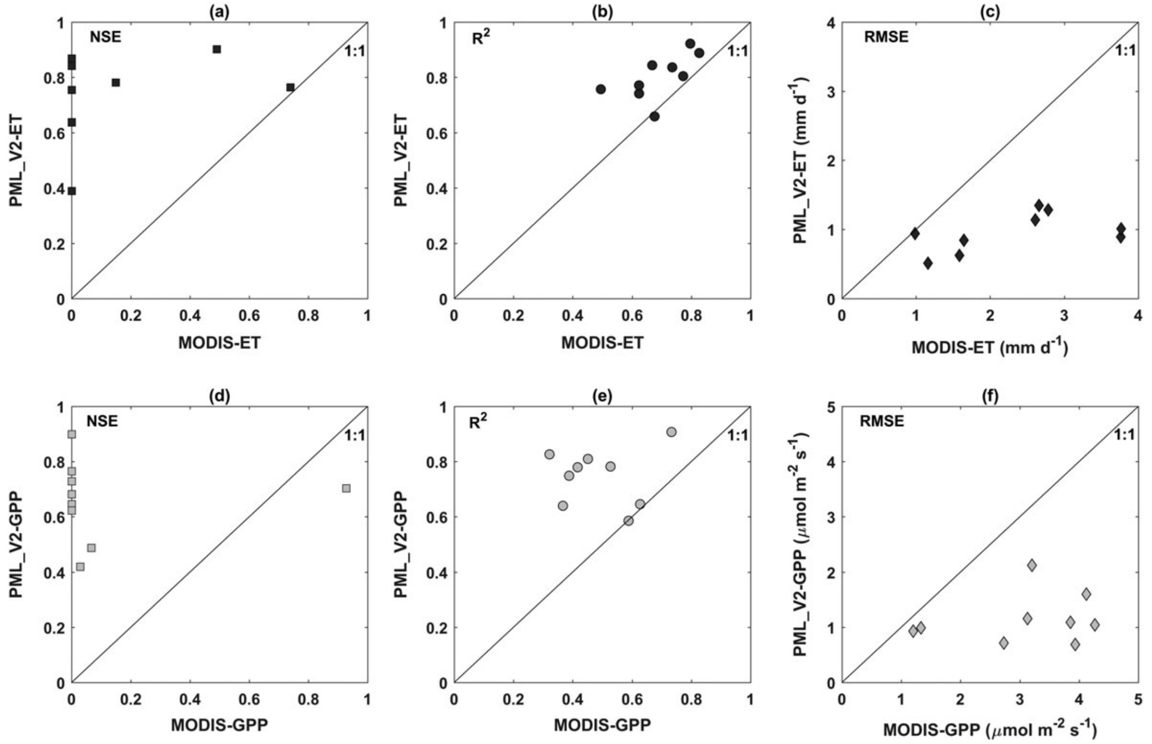

FIGURE 7 Statistic comparison of PML_V2 model (in validation mode) and MODIS products at nine Australian flux sites. Nash–Sutcliffe efficiency (NSE), R^2, and root mean square error (RMSE) are given for ET (a–c) as black and GPP (d–f) as shaded symbols, respectively. For visualization, the negative NSE values of MODIS products in (a) and (d) are set to zero indicating poor model performance

TABLE 4 PML_V2 performance in prediction mode compared with the published at two flux sites How and Tum, in terms of the coefficient of determination (R^2) and root mean square error (RMSE)

			How				Tum			
			ET	ET	GPP	GPP	ET	ET	GPP	GPP
Reference	Temporal period	Temporal resolution	R^2	RMSE mm d^{-1}	R^2	RMSE µmol m^{-2} s^{-1}	R^2	RMSE mm d^{-1}	R^2	RMSE µmol m^{-2} s^{-1}
This study	2001–2012	8 days	0.76	1.01	0.75	1.04	0.84	0.84	0.81	1.09
Yebra et al. (2015, 2013)	2001–2006	16 days (ET)8 days (GPP)	0.79	0.14	0.76	1.17	0.68	0.52	0.53	1.85
Hu et al. (2017)	2001–2006	8 days	0.67	0.90	0.57	1.79	0.85	0.84	0.78	2.43

et al., 1995; Thornley, 1976, 1998a). Compared with the eddy covariance observations, the PML_V2 model yields satisfactory estimates of ET and GPP in general (Figures 3 and 4), with slightly better performance for ET than GPP detected (Figures 3 and 5). This could be a result of the following factors. First, available energy is the foremost environmental driving variable triggering stomatal activities, rather than CO_2 concentration. The PML_V2 model kept the energy-driven response of stomata to multiple environmental variables, yet the photosynthesis model was introduced. This induces a lower model sensitivity of simulating ET with the energy driven G_c formula, in which GPP was calculated as a relatively weak carbon constrain. Second, regarding the two components of ET, transpiration through stomata in the PML_V2 model depends on canopy interaction with the atmosphere, whereas soil evaporation is not related to stomatal behaviour. The uncertainty of estimated transpiration from the carbon constraint is mitigated by evaluating total ET as the sum of transpiration and soil evaporation. Third, GPP is controlled not only by PAR and temperature but also other environmental factors such as soil moisture (Cleverly, Eamus, Luo, et al., 2016; Eamus et al., 2013) and atmospheric CO_2 concentration (Donohue, Roderick, McVicar, & Farquhar, 2013), which is not explicitly considered in the present PML_V2 model due to model simplicity and data availability concern. However, among the nine flux sites used in our study, seven of which are located in warm and arid environments where the ecosystems are water limited (Figures 4 and 5). Vegetation in these ecosystems relies on water availability and may have developed deep root system to support growth during relatively short dry period. This can be an explanation for less satisfactory model performance at the nonforest sites, where high GPP periods are underestimated by PML_V2. However, when precipitation remains extremely low, GPP is again water limited during long dry periods; yet the model lacks the water constraint in calculating GPP during these periods. Additionally, these warm and dry ecosystems are sensitive to variations in CO_2 concentration, yet which value is given as 380 µmol mol^{-1} across sites. As the study period is relatively short, this is a fair assumption but not for long-term pattern. The model performance is likely to be improved by introducing other environmental constraints such as precipitation and soil moisture into the model. At specific sites, the model well captured the GPP variation throughout the study period at evergreen broadleaf forests sites (i.e., Tum and Wom) but less so at OSH (ASM) and GRA (Stp and DaP) sites during both peak and low GPP periods. Considering the fact that the peaks at ASM and Stp were real (Cleverly et al., 2013; Eamus et al., 2013) and contribute greatly to the global carbon sink anomaly (Cleverly, Eamus, Restrepo Coupe, et al., 2016; Poulter et al., 2014), the less satisfactory model performance on high and low GPP values can be explained as a result of using NSE as the objective function to parameterize the PML_V2 model (Equations 8–10). NSE could induce suboptimal solutions when the data set contains extremely large values. For ASM, with only 2 years data available, extreme high GPP observations at the beginning of 2011 can cause large uncertainties in model performance, thus bring large bias for GPP peaks in wet season and minima in dry season (Figure 5). For Stp and DaP, extreme low GPP observations occur repeatedly each year and, hence, jeopardize the overall model performance. Additionally, the photosynthesis principles adopted in PML_V2 model are relatively simple and empirical (rectangular hyperbola), which generally accounts for C_3 rather than C_4 species. Despite there is a fair difference between C_3 and C_4 assimilation process, and some of the nonforest sites are partly C_4 grass dominated, the model fails to distinguish this difference thus lead to poor results at these sites. Further investigation is required to test how and to what level would the biological process influence modelled ET and GPP.

It is also noted that we adopted the big-leaf scaling-up method to obtain canopy level carbon uptake and conductance, which could induce uncertainty in estimating ET and GPP due to scaling effect. In fact, there is a diffuse difference of radiation between sunlit and shaded leaves, which means that the water vapour flux and assimilation rate can vary greatly between the these two type of leaves, and the effect is detectable at canopy level (Irmak et al., 2008; Zhang, Liu, Xu, Cai, & Li, 2011). This difference is neglected in the big-leaf approach thus bring uncertainty for simulating ET and GPP. The canopy heterogeneity at both horizontal and vertical direction also means the bulk canopy conductance, and assimilation is not simply the sum of the leaf level water loss and carbon gain. However, differentiating sunlit and shade leaves will bring more complex model structure and more parameters, which definitely influences model parameterization and applicability.

6 | CONCLUSIONS

This study developed a coupled PML_V2 model to estimate evapotranspiration and carbon assimilation using a relatively simple structure while retaining reasonable biophysical significance. The model was examined against observations from nine flux sites that cover a wide range of climate and biome types in Australia. The model performed well in both ET and GPP simulation at 8-day temporal scale. Sensitivity analysis and validation experiment as well as comparison with other modelled results further demonstrate that the proposed PML_V2 model is good for estimating ecosystem water and carbon fluxes. This is an ongoing study. We are testing its performance in other parts of world and integrating the PML_V2 model into catchment hydrological modelling for broader ecological and hydrological applications from catchment to region.

ACKNOWLEDGEMENTS

The first author acknowledges the Chinese Scholarship Council for supporting her PhD study at University of Technology Sydney and CSIRO Land and Water. We thank the researchers at the OzFlux sites and MODIS project for allowing the use of the water flux, carbon flux meteorological, and remote sensing data used in this study. Dongdong Kong provided technical help for programming and data processing. Data used for modelling are properly cited, and data generated by PML_V2 model are freely available upon request from the first author (Rong Gan, email: rong.gan@csiro.au) or the corresponding author (Yongqiang Zhang, email: yongqiang.zhang@csiro.au). The authors declare no conflict of interest.

ORCID

Yongqiang Zhang http://orcid.org/0000-0002-3562-2323

REFERENCES

Baldocchi, D. D., Luxmoore, R. J., & Hatfield, J. L. (1991). Discerning the forest from the trees: An essay on scaling canopy stomatal conductance. *Agricultural and Forest Meteorology*, *54*, 197–226. https://doi.org/10.1016/0168-1923(91)90006-C

Ball, J. T., Woodrow, I. E., & Berry, J. A. (1987). A model predicting stomatal conductance and its contribution to the control of photosynthesis under different environmental conditions. In *Progress in photosynthesis research* (pp. 221–224). Springer. doi:citeulike-article-id:8423355

Bastiaanssen, W. G. M., Menenti, M., Feddes, R. A., & Holtslag, A. A. M. (1998). A remote sensing surface energy balance algorithm for land (SEBAL): 1. Formulation. *Journal of Hydrology*, *212–213*, 198–212. https://doi.org/10.1016/S0022-1694(98)00253-4

Bastiaanssen, W. G. M., Pelgrum, H., Wang, J., Ma, Y., Moreno, J. F., Roerink, G. J., & Van Der Wal, T. (1998). A remote sensing surface energy balance algorithm for land (SEBAL): 2. Validation. *Journal of Hydrology*, *212–213*, 213–229. https://doi.org/10.1016/S0022-1694(98)00254-6

Beer, C., Reichstein, M., Tomelleri, E., Ciais, P., Jung, M., Carvalhais, N., … Papale, D. (2010). Terrestrial gross carbon dioxide uptake: Global distribution and covariation with climate. *Science*, *329*(5993), 834–838.

Beringer, J., Hutley, L. B., McHugh, I., Arndt, S. K., Campbell, D., Cleugh, H. A., … Wardlaw, T. (2016). An introduction to the Australian and New Zealand flux tower network—OzFlux. *Biogeosciences*, *13*, 5895–5916. https://doi.org/10.5194/bg-13-5895-2016

Bonan, G. B., Oleson, K. W., Fisher, R. A., Lasslop, G., & Reichstein, M. (2012). Reconciling leaf physiological traits and canopy flux data: Use of the TRY and FLUXNET databases in the community land model version 4. *Journal of Geophysical Research – Biogeosciences*, *117*, 1–19. https://doi.org/10.1029/2011JG001913

Bonan, G. B., Williams, M., Fisher, R. A., & Oleson, K. W. (2014). Modeling stomatal conductance in the earth system: Linking leaf water-use efficiency and water transport along the soil-plant-atmosphere continuum. *Geoscientific Model Development*, *7*, 2193–2222. https://doi.org/10.5194/gmd-7-2193-2014

Bruhn, D., Mikkelsen, T. N., Herbst, M., Kutsch, W. L., Ball, M. C., & Pilegaard, K. (2011). Estimating daytime ecosystem respiration from eddy-flux data. *Biosystems*, *103*, 309–313. https://doi.org/10.1016/j.biosystems.2010.10.007

Campbell, G. S., & Norman, J. M. (1998). *An introduction to environmental biophysics* (2nd ed.). New York: Springer-Verlag.

Chen, J., Liu, J., Cihlar, J., & Goulden, M. (1999). Daily canopy photosynthesis model through temporal and spatial scaling for remote sensing applications. *Ecological Modelling*, *124*, 99–119. https://doi.org/10.1016/S0304-3800(99)00156-8

Cleugh, H. A., Leuning, R., Mu, Q., & Running, S. W. (2007). Regional evaporation estimates from flux tower and MODIS satellite data. *Remote Sensing of Environment*, *106*, 285–304. https://doi.org/10.1016/j.rse.2006.07.007

Cleverly, J., Boulain, N., Villalobos-Vega, R., Grant, N., Faux, R., Wood, C., … Eamus, D. (2013). Dynamics of component carbon fluxes in a semi-arid Acacia woodland, central Australia. *Journal of Geophysical Research – Biogeosciences*, *118*, 1168–1185. https://doi.org/10.1002/jgrg.20101

Cleverly, J., Eamus, D., Luo, Q., Restrepo Coupe, N., Kljun, N., Ma, X., … Huete, A. (2016). The importance of interacting climate modes on Australia's contribution to global carbon cycle extremes. *Scientific Reports*, *6*, 23113. https://doi.org/10.1038/srep23113

Cleverly, J., Eamus, D., Restrepo Coupe, N., Chen, C., Maes, W., Li, L., … Huete, A. (2016). Soil moisture controls on phenology and productivity in a semi-arid critical zone. *Science of the Total Environment*, *568*, 1227–1237. https://doi.org/10.1016/j.scitotenv.2016.05.142

Collatz, G. J., Ball, J. T., Grivet, C., & Berry, J. A. (1991). Physiological and environmental regulation of stomatal conductance, photosynthesis and transpiration: A model that includes a laminar boundary layer. *Agricultural and Forest Meteorology*, *54*, 107–136. https://doi.org/10.1016/0168-1923(91)90002-8

Cox, P., Huntingford, C., & Harding, R. (1998). A canopy conductance and photosynthesis model for use in a GCM land surface scheme. *Journal of Hydrology*, *212–213*, 79–94. https://doi.org/10.1016/S0022-1694(98)00203-0

Dai, Y., Dickinson, R. E., Wang, Y.-P. P., Al, D. A. I. E. T., Dai, Y., Dickinson, R. E., & Wang, Y.-P. P. (2004). A two-big-leaf model for canopy temperature, photosynthesis, and stomatal conductance. *Journal of Climate*, *17*, 2281–2299. https://doi.org/10.1175/1520-0442(2004)017<2281:ATMFCT>2.0.CO;2

De Kauwe, M. G., Kala, J., Lin, Y. S., Pitman, A. J., Medlyn, B. E., Duursma, R. A., … Miralles, D. G. (2015). A test of an optimal stomatal conductance scheme within the CABLE land surface model. *Geoscientific Model Development*, *8*, 431–452. https://doi.org/10.5194/gmd-8-431-2015

Donohue, R. J., Roderick, M. L., McVicar, T. R., & Farquhar, G. D. (2013). Impact of CO2 fertilization on maximum foliage cover across the globe's warm, arid environments. *Geophysical Research Letters*, *40*, 3031–3035. https://doi.org/10.1002/grl.50563

Eamus, D., Cleverly, J., Boulain, N., Grant, N., Faux, R., & Villalobos-Vega, R. (2013). Carbon and water fluxes in an arid-zone Acacia savanna woodland: An analyses of seasonal patterns and responses to rainfall events. *Agricultural and Forest Meteorology*, *182–183*, 225–238. https://doi.org/10.1016/j.agrformet.2013.04.020

Ershadi, A., McCabe, M. F., Evans, J. P., Chaney, N. W., & Wood, E. F. (2014). Multi-site evaluation of terrestrial evaporation models using FLUXNET data. *Agricultural and Forest Meteorology*, *187*, 46–61. https://doi.org/10.1016/j.agrformet.2013.11.008

Farquhar, G. D., & Sharkey, T. D. (1982). Stomatal conductance and photosynthesis. *Annual Review of Plant Physiology*, *33*, 317–345. https://doi.org/10.1146/annurev.pp.33.060182.001533

Farquhar, G. D., von Caemmener, S., & Berry, J. A. (1980). A biochemical model of photosynthesis CO2 fixation in leaves of C3 species. *Planta*, *149*, 78–90.

Farquhar, G. D., & von Caemmerer, S. (1892). Modelling of photosynthetic response to environmental conditions. *Physiological Plant Ecology II*, 550–583.

Fisher, J. B., Tu, K. P., & Baldocchi, D. D. (2008). Global estimates of the land-atmosphere water flux based on monthly AVHRR and ISLSCP-II data, validated at 16 FLUXNET sites. *Remote Sensing of Environment*, *112*, 901–919. https://doi.org/10.1016/j.rse.2007.06.025

Granier, A., Biron, P., & Lemoine, D. (2000). Water balance, transpiration and canopy conductance in two beech stands. *Agricultural and Forest Meteorology*, *100*, 291–308. https://doi.org/10.1016/S0168-1923(99)00151-3

Guerschman, J. P., Van Dijk, A. I. J. M., Mattersdorf, G., Beringer, J., Hutley, L. B., Leuning, R., … Sherman, B. S. (2009). Scaling of potential evapotranspiration with MODIS data reproduces flux observations and catchment water balance observations across Australia. *Journal of Hydrology*, *369*, 107–119. https://doi.org/10.1016/j.jhydrol.2009.02.013

Hirose, T. (2005). Development of the Monsi-Saeki theory on canopy structure and function. *Annals of Botany*, *95*, 483–494. https://doi.org/10.1093/aob/mci047

Hu, Z., Wu, G., Zhang, L. L., Li, S., Zhu, X., Zheng, H., … Yu, G. (2017). Modeling and partitioning of regional evapotranspiration using a satellite-driven water-carbon coupling model. *Remote Sensing*, *9*, 1–5. https://doi.org/10.3390/rs9010054

Irmak, S., Mutiibwa, D., Irmak, A., Arkebauer, T. J., Weiss, A., Martin, D. L., & Eisenhauer, D. E. (2008). On the scaling up leaf stomatal resistance to canopy resistance using photosynthetic photon flux density. *Agricultural and Forest Meteorology*, *148*, 1034–1044. https://doi.org/10.1016/j.agrformet.2008.02.001

Isaac, P., Cleverly, J., McHugh, I., van Gorsel, E., Ewenz, C., & Beringer, J. (2016). OzFlux data: Network integration from collection to curation. *Biogeosciences Discussions*, 1–41. https://doi.org/10.5194/bg-2016-189

Jarvis, P. G. (1976). The interpretation of the variations in leaf water potential and stomatal conductance found in canopies in the field. *Philosophical Transactions of the Royal Society B*, *273*, 593–610. https://doi.org/10.1098/rstb.1976.0035

Jasechko, S., Sharp, Z. D., Gibson, J. J., Birks, S. J., Yi, Y., & Fawcett, P. J. (2013). Terrestrial water fluxes dominated by transpiration. *Nature*, *496*, 347–350. https://doi.org/10.1038/nature11983

Jönsson, P., & Eklundh, L. (2004). TIMESAT—A program for analyzing time-series of satellite sensor data. *Computational Geosciences*, *30*, 833–845. https://doi.org/10.1016/j.cageo.2004.05.006

Kattge, J., & Knorr, W. (2007). Temperature acclimation in a biochemical model of photosynthesis: A reanalysis of data from 36 species. *Plant, Cell and Environment*, *30*, 1176–1190. https://doi.org/10.1111/j.1365-3040.2007.01690.x

Katul, G. G., Ellsworth, D. S., & Lai, C. T. (2000). Modelling assimilation and intercellular CO2 from measured conductance: A synthesis of approaches. *Plant, Cell and Environment*, *23*, 1313–1328. https://doi.org/10.1046/j.1365-3040.2000.00641.x

Katul, G., Manzoni, S., Palmroth, S., & Oren, R. (2010). A stomatal optimization theory to describe the effects of atmospheric CO2 on leaf photosynthesis and transpiration. *Annals of Botany*, *105*, 431–442. https://doi.org/10.1093/aob/mcp292

Kelliher, F. M., Leuning, R., Raupach, M. R., & Schulze, E. D. (1995). Maximum conductences for evaporation from global vegetation types. *Agricultural and Forest Meteorology*, *1923*, 1–14.

Kowalczyk, E. A., Wang, Y. P., & Law, R. M. (2006). The CSIRO atmosphere biosphere land exchange (CABLE) model for use in climate models and as an offline model. *CSIRO Marine and Atmospheric Research Paper*, *13*, 42. doi:1921232390

Leuning, R. (1995). A critical appraisal of a combined stomatal-photosynthesis model for C3 plants. *Plant, Cell & Environment*, *18*, 339–355. https://doi.org/10.1111/j.1365-3040.1995.tb00370.x

Leuning, R., Cleugh, H. A., Zegelin, S. J., & Hughes, D. (2005). Carbon and water fluxes over a temperate Eucalyptus forest and a tropical wet/dry savanna in Australia: Measurements and comparison with MODIS remote sensing estimates. *Agricultural and Forest Meteorology*, *129*, 151–173. https://doi.org/10.1016/j.agrformet.2004.12.004

Leuning, R., Zhang, Y. Q., Rajaud, A., Cleugh, H., & Tu, K. (2008). A simple surface conductance model to estimate regional evaporation using MODIS leaf area index and the Penman-Monteith equation. *Water Resources Research*, *44*, W10419. https://doi.org/10.1029/2007WR006562

Liu, Z., Wu, C., & Wang, S. (2017). Predicting forest evapotranspiration by coupling carbon and water cycling based on a critical stomatal conductance model. *IEEE Xplore: IEEE Transactions on Geoscience and Remote Sensing*, 1–9. https://doi.org/10.1109/JSTARS.2017.2715077

Long, D., & Singh, V. P. (2012). A two-source trapezoid model for evapotranspiration (TTME) from satellite imagery. *Remote Sensing of Environment*, *121*, 370–388. https://doi.org/10.1016/j.rse.2012.02.015

Ma, X., Huete, A., Yu, Q., Restrepo-Coupe, N., Beringer, J., Hutley, L. B., … Eamus, D. (2014). Parameterization of an ecosystem light-use-efficiency model for predicting savanna GPP using MODIS EVI. *Remote Sensing of Environment*, *154*, 253–271. https://doi.org/10.1016/j.rse.2014.08.025

Mallick, K., Boegh, E., Trebs, I., Alfieri, J. G., Kustas, W. P., Prueger, J. H., … Jarvis, A. J. (2015). Reintroducing radiometric surface temperature into the Penman-Monteith formulation. *Water Resources Research*, *51*, 6214–6243. https://doi.org/10.1002/2014WR016106

McVicar, T. R., & Jupp, D. L. B. (2002). Using covariates to spatially interpolate mositure availability in the Murray–Darling Basin: A novel use of remotel sensed data. *Remote Sensing of Environment*, *79*, 199–212.

Medlyn, B. E., Duursma, R. A., Eamus, D., Ellsworth, D. S., Prentice, I. C., Barton, C. V. M., … Wingate, L. (2011). Reconciling the optimal and empirical approaches to modelling stomatal conductance. *Global Change Biology*, *17*, 2134–2144. https://doi.org/10.1111/j.1365-2486.2010.02375.x

Monteith, J. L. (1965). Evaporation and environment. *Symposia of the Society for Experimental Biology*, *19*, 205–234. https://doi.org/10.1613/jair.301

Morales, P., Sykes, M. T., Prentice, I. C., Smith, P., Smith, B., Bugmann, H., … Ogee, J. (2005). Comparing and evaluating process-based ecosystem model predictions of carbon and water fluxes in major European forest biomes. *Global Change Biology*, *11*, 2211–2233. https://doi.org/10.1111/j.1365-2486.2005.01036.x

Morillas, L., Leuning, R., Villagarcía, L., García, M., Serrano-Ortiz, P., & Domingo, F. (2013). Improving evapotranspiration estimates in Mediterranean drylands: The role of soil evaporation. *Water Resources Research*, *49*, 6572–6586. https://doi.org/10.1002/wrcr.20468

Mu, Q., Heinsch, F. A., Zhao, M., & Running, S. W. (2007). Development of a global evapotranspiration algorithm based on MODIS and global meteorology data. *Remote Sensing of Environment*, *111*, 519–536. https://doi.org/10.1016/j.rse.2007.04.015

Mu, Q., Zhao, M., & Running, S. W. (2011). Improvements to a MODIS global terrestrial evapotranspiration algorithm. *Remote Sensing of Environment*, *115*, 1781–1800. https://doi.org/10.1016/j.rse.2011.02.019

Norman, J. M., Kustas, W. P., & Humes, K. S. (1995). A two-source approach for estimating soil and vegetation energy fluxes from observations of directional radiometric surface temperature. *Agricultural and Forest Meteorology*, *77*, 263–293. https://doi.org/10.1016/0168-1923(95)02265-Y

Oleson, K.W., Lawrence, D.M., Gordon, B., Flanner, M.G., Kluzek, E., Peter, J., …, Zeng, X., 2010. Technical description of version 4. 0 of the community land model (CLM). NCAR Tech. Note.

Papale, D., Reichstein, M., Aubinet, M., Canfora, E., Bernhofer, C., Kutsch, W., … Yakir, D. (2006). Towards a standardized processing of net ecosystem exchange measured with eddy covariance technique: Algorithms and uncertainty estimation. *Biogeosciences*, *3*, 571–583. https://doi.org/10.5194/bg-3-571-2006

Papale, D., & Valentini, R. (2003). A new assessment of European forests carbon exchanges by eddy fluxes and artificial neural network spatialization. *Global Change Biology*, *9*, 525–535. https://doi.org/10.1046/j.1365-2486.2003.00609.x

Poulter, B., Frank, D., Ciais, P., Myneni, R. B., Andela, N., Bi, J., … van der Werf, G. R. (2014). Contribution of semi-arid ecosystems to interannual variability of the global carbon cycle. *Nature*, *509*, 600–603. https://doi.org/10.1038/nature13376

Priestley, C. H. B., & Taylor, R. J. (1972). On the assessment of surface heat flux and evaporation using large-scale parameters. In *Monthly weather review* (pp. 81–92). https://doi.org/10.1175/1520-0493(1972)100<0081:OTAOSH>2.3.CO;2

Reichstein, M., Falge, E., Baldocchi, D., Papale, D., Aubinet, M., Berbigier, P., … Valentini, R. (2005). On the separation of net ecosystem exchange into assimilation and ecosystem respiration: Review and improved algorithm. *Global Change Biology*, *11*, 1424–1439. https://doi.org/10.1111/j.1365-2486.2005.001002.x

Running, S. W., & Coughlan, J. C. (1988). A general model of forest ecosystem processes for regional applications I. Hydrologic balance, canopy gas exchange and primary production processes. *Ecological Modelling*, *42*, 125–154. https://doi.org/10.1016/0304-3800(88)90112-3

Running, S. W., Nemani, R. R., Heinsch, F. A., Zhao, M., Reeves, M., & Hashimoto, H. (2004). A continuous satellite-derived measure of global terrestrial primary production. *Bioscience*, *54*, 547–560.

Sellers, P. J. (1997). Modeling the exchanges of energy, water, and carbon between continents and the atmosphere. *Science*, *275*(80), 502–509. https://doi.org/10.1126/science.275.5299.502

Sellers, P. J., Randall, D. A., Collatz, G. J., Berry, J. A., Field, C. B., Dazlich, D. A., … Bounoua, L. (1996). A revised land surface parameterization (SiB2) for atmospheric GCMs. *Part I: Model formulation Journal of Climate*, *9*, 676–705. https://doi.org/10.1175/1520-0442(1996)009<0676:ARLSPF>2.0.CO;2

Shi, H., Li, L., Eamus, D., Cleverly, J., Huete, A., Beringer, J., … Hutley, L. (2014). Intrinsic climate dependency of ecosystem light and water-use-efficiencies across Australian biomes. *Environmental Research Letters*, *9*, 104002. https://doi.org/10.1088/1748-9326/9/10/104002

Stewart, J. B. (1988). Modelling surface conductance of pine forest. *Agricultural and Forest Meteorology*, *43*, 19–35. https://doi.org/10.1016/0168-1923(88)90003-2

Thornley, J. H. M. (1976). *Mathematical models in plant physiology: A quantitative approach to problems in plant and crop physiology*, *Experimental botany; v. 8*. London; New York: Academic Press.

Thornley, J. H. M. (1998a). Dynamic model of leaf photosynthesis with acclimation to light and nitrogen. *Annals of Botany*, *81*, 421–430. https://doi.org/10.1006/anbo.1997.0575

Thornley, J. H. M. (1998b). Temperature and CO_2 responses of leaf and canopy photosynthesis: A clarification using the non-rectangular hyperbola model of photosynthesis. *Annals of Botany*, *82*, 883–892. https://doi.org/10.1006/anbo.1998.0777

Tuzet, A., Perrier, A., & Leuning, R. (2003). A coupled model of stomatal conductance, photosynthesis and transpiration. *Plant, Cell and Environment*, *26*, 1097–1116. https://doi.org/10.1046/j.1365-3040.2003.01035.x

Van Gorsel, E., Wolf, S., Cleverly, J., Isaac, P., Haverd, V., Ewenz, C., … Silberstein, R. (2016). Carbon uptake and water use in woodlands and forests in southern Australia during an extreme heat wave event in the “angry Summer” of 2012/2013. *Biogeosciences*, *13*, 5947–5964. https://doi.org/10.5194/bg-13-5947-2016

Wang, K., & Dickinson, R. E. (2012). A review of global terrestrial evapotranspiration: Observation, modeling, climatology, and climatic variability. *Reviews of Geophysics*, *50*. https://doi.org/10.1029/2011RG000373

Wang, Y. P., Kowalczyk, E., Leuning, R., Abramowitz, G., Raupach, M. R., Pak, B., … Luhar, A. (2011). Diagnosing errors in a land surface model (CABLE) in the time and frequency domains. J. Geophys. Res. *Biogeosciences*, *116*. https://doi.org/10.1029/2010JG001385

Wilson, K., Goldstein, A., Falge, E., Aubinet, M., Baldocchi, D., Berbigier, P., … Verma, S. (2002). Energy balance closure at FLUXNET sites. *Agricultural and Forest Meteorology*, *113*, 223–243. https://doi.org/10.1016/S0168-1923(02)00109-0

Yang, Y., Donohue, R. J., McVicar, T. R., & Roderick, M. L. (2015). An analytical model for relating global terrestrial carbon assimilation with climate and surface conditions using a rate limitation framework. *Geophysical Research Letters*, *42*, 9825–9835. https://doi.org/10.1002/2015GL066835

Yang, Y., Long, D., & Shang, S. (2013). Remote estimation of terrestrial evapotranspiration without using meteorological data. *Geophysical Research Letters*, *40*, 3026–3030. https://doi.org/10.1002/grl.50450

Yebra, M., Van Dijk, A. I. J. M. J. M., Leuning, R., & Guerschman, J. P. (2015). Global vegetation gross primary production estimation using satellite-derived light-use efficiency and canopy conductance. *Remote Sensing of Environment*, *163*, 206–216. https://doi.org/10.1016/j.rse.2015.03.016

Yebra, M., Van Dijk, A., Leuning, R., Huete, A., & Guerschman, J. P. (2013). Evaluation of optical remote sensing to estimate actual evapotranspiration and canopy conductance. *Remote Sensing of Environment*, *129*, 250–261. https://doi.org/10.1016/j.rse.2012.11.004

Yu, Q., Goudriaan, J., & Wang, T. D. (2001). Modelling diurnal courses of photosynthesis and transpiration of leaves on the basis of stomatal and non-stomatal responses, including photoinhibition. *Photosynthetica*, *39*, 43–51. https://doi.org/10.1023/A:1012435717205

Yu, Q., Zhang, Y., Liu, Y., & Shi, P. (2004). Simulation of the stomatal conductance of winter wheat in response to light, temperature and CO2 changes. *Annals of Botany*, *93*, 435–441. https://doi.org/10.1093/aob/mch023

Zhang, Y., Chiew, F., Peña-Arancibia, J., Sun, F., Li, H., & Leuning, R. (2017). Global variation of transpiration and soil evaporation and the role of their major climate drivers. *Journal of Geophysical Research – Atmospheres*, *122*, 6868–6881. https://doi.org/10.1002/2017JD027025

Zhang, Y. Q., Chiew, F. H. S., Zhang, L., Leuning, R., & Cleugh, H. A. (2008). Estimating catchment evaporation and runoff using MODIS leaf area index and the Penman-Monteith equation. *Water Resources Research*, *44*, 1–15. https://doi.org/10.1029/2007WR006563

Zhang, Y., Chiew, F. H. S., Zhang, L., & Li, H. (2009). Use of remotely sensed actual evapotranspiration to improve rainfall–runoff modeling in Southeast Australia. *Journal of Hydrometeorology*, *10*, 969–980. https://doi.org/10.1175/2009JHM1061.1

Zhang, Y., Leuning, R., Hutley, L. B., Beringer, J., McHugh, I., & Walker, J. P. (2010). Using long-term water balances to parameterize surface conductances and calculate evaporation at 0.05 spatial resolution. *Water Resources Research*, *46*, W05512. https://doi.org/10.1029/2009WR008716

Zhang, B., Liu, Y., Xu, D., Cai, J., & Li, F. (2011). Evapotranspiraton estimation based on scaling up from leaf stomatal conductance to canopy conductance. *Agricultural and Forest Meteorology*, *151*, 1086–1095. https://doi.org/10.1016/j.agrformet.2011.03.012

Zhang, Y., Peña-Arancibia, J. L., McVicar, T. R., Chiew, F. H. S., Vaze, J., Liu, C., … Pan, M. (2016). Multi-decadal trends in global terrestrial evapotranspiration and its components. *Scientific Reports*, *6*, 19124. https://doi.org/10.1038/srep19124

Zhang, Y., & Wegehenkel, M. (2006). Integration of MODIS data into a simple model for the spatial distributed simulation of soil water content and. *Remote Sensing of Environment*, *104*, 393–408. https://doi.org/10.1016/j.rse.2006.05.011

Zhou, Y., Zhang, Y., Vaze, J., Lane, P., & Xu, S. (2015). Impact of bushfire and climate variability on streamflow from forested catchments in southeast Australia. *Hydrology and Earth System Sciences Discussions*, *10*, 4397–4437. https://doi.org/10.5194/hessd-10-4397-2013

Zhu, Z., Piao, S., Myneni, R. B., Huang, M., Zeng, Z., Canadell, J. G., … Poulter, B. (2016). Greening of the Earth and its drivers. *Nature Climate Change*, *6*. early online. doi:https://doi.org/10.1038/NCLIMATE3004

How to cite this article: Gan R, Zhang Y, Shi H, et al. Use of satellite leaf area index estimating evapotranspiration and gross assimilation for Australian ecosystems. *Ecohydrology*. 2018;11:e1974. https://doi.org/10.1002/eco.1974

APPENDIX A

The canopy conductance G_c in the PML_V2 model is deduced from stomatal conductance as follows:

The widely used Ball–Berry g_s model (Ball et al., 1987) was developed from leaf gas exchange experiments as

$$g_s = g_0 + m\frac{A_n h_s}{C_s}, \tag{A1}$$

where g_0 is the value of g_s at the light compensation point (mol m^{-2} s^{-1}), m is stomatal conductance coefficient, C_s is leaf surface CO$_2$ concentration (μmol mol^{-1}), h_s is relative humidity, and A_n is net assimilation rate (μmol m^{-2} s^{-1}). As stomata response to leaf surface VPD (D_s) rather than h_s, Leuning (1995) replaced h_s in Equation A1 with a hyperbolic constrain of D_s to g_s and gave

$$g_s = g_0 + m\frac{A_n}{(C_s - \Gamma)(1 + D_s/D_0)}, \tag{A2}$$

in which Γ is CO$_2$ compensation concentration (μmol mol^{-1}) and D_0 is a parameter that represents the sensitivity of g_s to D_s. Note that above mentioned g_s models (Equations A1 and A2) simulate stomatal conductance to carbon flux, and the stomatal conductance to water vapour can be approximated as 1.6 times of that to carbon flux (Medlyn et al., 2011; Yebra et al., 2015).

To obtain g_s according to Equations A1 or A2, the biochemical photosynthesis model developed by Farquhar, von Caemmener, and Berry (1980) is commonly implemented to calculate A_n, in which the rate of CO$_2$ uptake is limited either by Rubisco activity (J_c), electron transport (J_e), or exportation or utilization capacity of photosynthetic products (J_s; Collatz et al., 1991). Although this method is widely used, parameters of this model are difficult to obtain, and the description of the underlying processes remains elusive (Thornley, 1998b).

On the aware of practicability of the model, we therefore intend to develop a simple and coupled G_c model based on gross photosynthesis and stomatal response. According to Yu, Goudriaan, and Wang (2001), considering the fact that g_s increases immediately with light incidence, A_n should be replaced by gross assimilation rate (A_g, μmol m^{-2} s^{-1}) and use C_s instead of C_s–Γ in Equation A2. Additionally, A_g and g_o goes to zero in dark, D_s, and C_s can be approximated using D_a and C_a, respectively; Yu et al. (2004) suggests that g_s can be written as a function of A_g, C_a, and D_a at leaf level as

$$g_s = m\frac{A_g}{C_a(1 + D_a/D_0)}, \tag{A3}$$

in which C_a is the atmospheric CO$_2$ concentration, the gross assimilation A_g is calculated following Thornley (1976) as a rectangular hyperbola function to both PAR and C_a as

$$A_g = \frac{A_m \alpha I \eta C_a}{A_m \alpha I + A_m \eta C_a + \alpha I \eta C_a}, \tag{A4}$$

where α is the initial slope of the light response curve to assimilation rate (i.e., quantum efficiency; μmol CO$_2$ [μmol PAR]$^{-1}$), η is the initial slope of the CO$_2$ response curve to assimilation rate (i.e., carboxylation efficiency; μmol m^{-2} s^{-1} [μmol m^{-2} s^{-1}]$^{-1}$), I is the incident flux of PAR (μmol m^{-2} s^{-1}), which is converted from PAR to photon flux assuming 4.6 μmol photons per Joule (Oleson et al., 2010), and A_m is the maximum photosynthetic rate obtained when both I and C_a are saturating (μmol m^{-2} s^{-1}).

Values of the light and carbon saturated rate of photosynthesis (A_m) are sensitive to species and can be reached either by Rubisco-limited J_c, electron-limited J_e, or transport-capacity-limited J_s in the Farquhar model (Farquhar & Sharkey, 1982), with the other environmental factors (e.g., water status) are assumed optimal (Thornley, 1998b). Given that the three limitation rates of assimilation (J_c, J_e, and J_s) are all directly or indirectly related to the maximum catalytic capacity of Rubisco ($V_{c,max}$), we simplify the photosynthesis model by using a notional capacity V_m, to represent A_m in Equation A4. As V_m is a kinetic parameter needs to be adjusted to temperature, it can be described by the equation (Campbell & Norman, 1998; Katul, Ellsworth, & Lai, 2000; Katul, Manzoni, Palmroth, & Oren, 2010):

$$V_m = \frac{V_{m,25}\exp[a(T-25)]}{1+\exp[b(T-41)]}, \tag{A5}$$

where $V_{m,25}$ is the value of V_m when T = 25 °C, T (°C) is temperature, a and b are temperature coefficients given as 0.031 and 0.115, respectively (Campbell & Norman, 1998). Note that the V_m introduced here is different from those used as $V_{c,max}$. At this point, Equation A3 can be rewritten into

$$g_s = m\frac{V_m\alpha I\eta}{V_m\alpha I + V_m\eta C_a + \alpha I\eta C_a}\frac{1}{1+D/D_0}. \tag{A6}$$

On the canopy scale, we can hence calculate gross assimilation rate ($A_{c,g}$) from Equation A4 and canopy conductance (G_c) from Equation A6 following the integration principle. The light extinction law $I = I_0 \exp(-kl)$ is adopted here to obtain

$$\begin{aligned} A_{c,g} = \int_0^{LAI} A_g dl = \frac{V_m\alpha\eta C_a}{k(V_m\alpha+\alpha\eta C_a)} \\ \left\{kLAI + ln\frac{(\alpha V_m+\alpha\eta C_a)I_0+\eta V_m C_a}{(\alpha V_m+\alpha\eta C_a)I_0\exp(-kLAI)+V_m\eta C_a}\right\}, \end{aligned} \tag{A7}$$

where I_0 is the flux density of PAR at the top of the canopy (μmol m^{-2} s^{-1}), l is the unit leaf area (m^2 m^{-2}), and $k = k_Q$ is the extinction coefficient. To simplify, we have

$$P_1 = V_m\alpha I_0\eta, \quad P_2 = V_m\alpha I_0, \quad P_3 = V_m\eta C_a, \quad P_4 = \alpha I_0\eta C_a. \tag{A8}$$

As a result, canopy gross assimilation rate or ecosystem GPP is simplified as

$$GPP = A_{c,g} = \frac{P_1 C_a}{k(P_2+P_4)}\left\{kLAI + ln\frac{P_2+P_3+P_4}{P_2+P_3\exp(kLAI)+P_4}\right\}. \tag{A9}$$

Furthermore, by integrating Equation A6 up to canopy level, one can obtain the following new G_c model:

$$\begin{aligned} G_c = \int_0^{LAI} g_s dl = m\frac{P_1}{k(P_2+P_4)} \\ \left\{kLAI + ln\frac{P_2+P_3+P_4}{P_2+P_3\exp(kLAI)+P_4}\right\}\frac{1}{1+D/D_0}. \end{aligned} \tag{A10}$$